scientific reports

Check for updates

OPEN

Pneumatophore CO_2 effluxes decrease with increased salinity in mangrove forests of Yucatan, Mexico

Julio A. Salas-Rabaza[1], Laura Yáñez-Espinosa[2], Eduardo Cejudo[3], Gabriela Cerón-Aguilera[1], Roberth Us-Santamaría[1] & José Luis Andrade[1]✉

Although mangrove forests are great carbon sinks, they also release carbon dioxide (CO_2) from soil, plants, and water through respiration. Many studies have focused on CO_2 effluxes only from soils, but the role of biogenic structures such as pneumatophore roots has been poorly studied. Hence, CO_2 effluxes from pneumatophores were quantified at sediment-air (non-flooded sediment) and water–air (flooded sediment) interfaces along a salinity gradient in three mangrove types (fringe, scrub, and basin) dominated by *Avicennia germinans* during the dry and rainy seasons in Yucatan, Mexico. Pneumatophore abundance explained up to 91% of CO_2 effluxes for scrub, 87% for fringe, and 83% for basin mangrove forests at the water–air interface. Overall, CO_2 effluxes were inversely correlated with temperature and salinity. The highest CO_2 effluxes were in the fringe and the lowest were in the scrub mangrove forests. Flooding decreased CO_2 effluxes from the dry to the rainy season in all mangrove forests. These results highlight the contribution of pneumatophores to mangrove respiration, and the need to include them in our current carbon budgets and models, but considering different exchange interfaces, seasons, and mangrove ecotypes.

Keywords *Avicennia germinans*, Carbon dioxide, Interface, Respiration, Roots

Mangrove forests are highly productive ecosystems with great potential as a blue carbon reservoir, particularly in the soil[1,2]. This is why these forests have been recognized as nature-based allies in climate change mitigation[3,4]. In soils, roots and microorganisms' respiration contributes to the main carbon output, as carbon dioxide (CO_2) efflux of forest ecosystems[5,6].

Plants, through respiration, utilize stored energy for growing and completing their lifecycle. Therefore, assessing plant respiration can deepen our understanding of mangrove tree physiology and their contribution to the ecosystem's carbon budget. In mangrove soils, several factors influencing CO_2 effluxes have been documented, such as temperature, salinity, and flooding[7–10]. However, many studies have focused on the quantification of soil CO_2 fluxes only, and a few have considered biogenic structures such as pneumatophores (root snorkels) and crab burrows, which could potentially increase CO_2[11–15] and methane emissions[16–20]. Pneumatophores have an internal pathway for gas flow, or aerenchyma[21–23], through which soil-produced gases can be emitted. Because of the presence of photosynthetic tissues and microalgae, they can carry out photosynthesis[24,25], which can lead to an additional source of oxygen for the anoxic soils. Pneumatophores represent a very important component of the carbon budget in mangrove forests, and their contribution to greenhouse gas emissions has already been reported[15,16,18,26].

Although mangrove forests are flooded at different times depending on regional seasonality and tidal regimes, CO_2 efflux at the water–air interface has been estimated in some cases[13,27], indicating that CO_2 effluxes are not negligible, especially during receding tides. Studies on these below-canopy CO_2 emissions should also consider the different mangrove ecological types, which vary in structure, composition, and carbon storage capacity. Also, because salinity and hydroperiod are the main drivers of mangrove zonation[28–31], high salinities and long

[1]Unidad de Recursos Naturales, Centro de Investigación Científica de Yucatán A.C., Calle 43 No. 130, Chuburná de Hidalgo, 97205 Mérida, Yucatan, Mexico. [2]Instituto de Investigación de Zonas Desérticas, Universidad Autónoma de San Luis Potosí, Altair No. 200, Col del Llano, 78377 San Luis Potosí, S.L.P., Mexico. [3]Unidad de Ciencias del Agua, Centro de Investigación Científica de Yucatán A.C., Calle 8, No. 39, Mz 29, SM 64, 77524 Cancún, Quintana Roo, Mexico. ✉email: andrade@cicy.mx

inundations decrease organic matter decomposition, which can ultimately be reduced by root respiration. In this study, we proposed quantifying CO_2 fluxes from soils and waters, with pneumatophores, along a salinity gradient in three different mangrove ecotypes (fringe, scrub, and basin) dominated by the black mangrove *Avicennia germinans* (L.) L. in the Yucatan Peninsula (Fig. 1), a region that has 60% of the total mangrove area in Mexico[32] and represents about 62% of all mangrove carbon stored in this country[31]. We hypothesized that CO_2 efflux magnitudes would be greater at high pneumatophore abundance because of the increased amount of living tissue that carries out respiration and of the aerenchyma that mobilizes the gases produced in soils. Also, effluxes would be higher at the sediment-air interface than at the water–air interface exchange because, in the former, aerobic microorganism respiration is also contained, and, in the latter, the water column exerts a physical barrier for gas diffusion from the sediment. Similarly, due to the sensitivity of CO_2 efflux to temperature and salinity[33,34], these CO_2 effluxes would be expected to increase at higher temperatures and lower salinities.

Results

Air and pneumatophores characterization

Mean air temperature was slightly higher during the dry season for all mangrove forests ($H = 97.64$; $P < 0.001$), but the greatest was for the scrub ecotype (dry, 31.98 ± 1.59 °C; rainy, 31.61 ± 2.26 °C; $P < 0.001$), which also had the highest temperatures of pneumatophores during the dry season (Table 1). Also, pneumatophores' dimensions

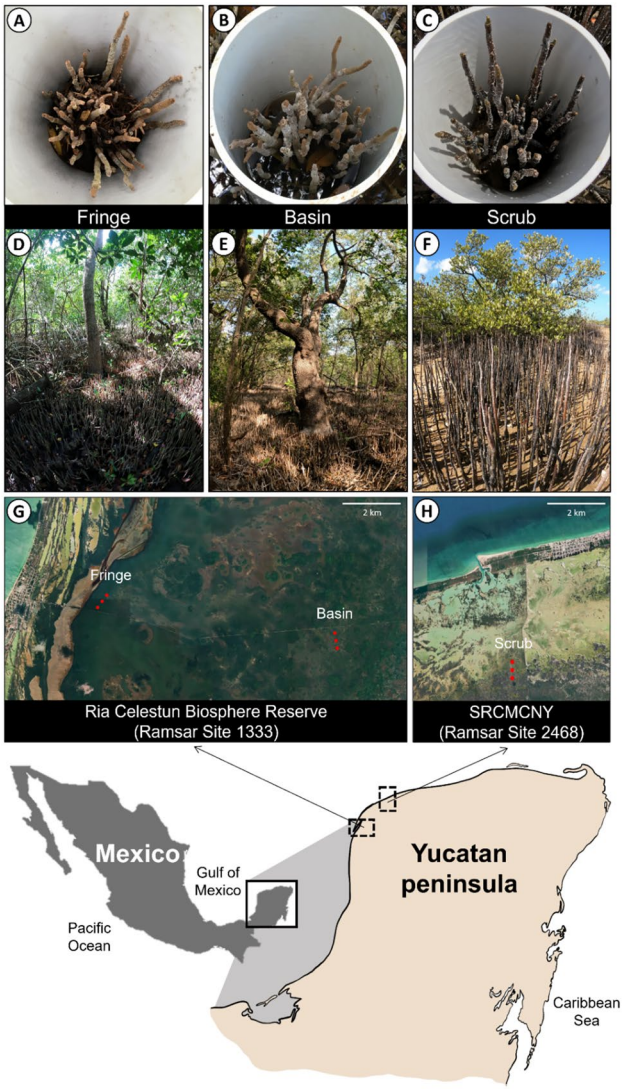

Figure 1. Location of the study sites in the Yucatan Peninsula. PVC tubes with pneumatophores where CO_2 efflux measurements were carried out (**A**–**C**), Mangrove ecotypes (**D**–**F**), and location of the mangrove ecotypes within the Ramsar sites (**G**, **H**). SRCMCNY = State Reserve Ciénagas y Manglares de la Costa Norte de Yucatán. Satellite images were obtained from Google Earth Pro 7.3 (https://earth.google.com) and maps were generated using Procreate Raster Graphics Program 5.3.9 (Savage Interactive Pty Ltd., https://procreate.com/procreate).

Variables	Basin		Fringe		Scrub		H-value
	Dry	Rainy	Dry	Rainy	Dry	Rainy	
Air temperature (°C)	29.53 ± 1.73^{b}	29.07 ± 1.87^{b}	28.69 ± 3.36^{bc}	26.96 ± 2.46^{c}	31.61 ± 2.26^{a}	31.98 ± 1.59^{a}	97.64*
Volumetric water content (m^3 H_2O m^{-3})	0.52 ± 0.01^{b}	0.55 ± 0.01^{a}	0.54 ± 0.01^{ab}	0.52 ± 0.01^{b}	0.56 ± 0.01^{a}	0.55 ± 0.01^{a}	110.49*
Surface water salinity (‰)	5.93 ± 1.33^{b}	1.9 ± 0.31^{c}	n.m	4.53 ± 0.54^{b}	36.39 ± 20.01^{a}	20 ± 13.13^{a}	62.75*
Pneu. abundance (pneu m^{-2})	256.01 ± 146.71^{a}	255.31 ± 144.58^{a}	255.3 ± 164.11^{a}	253.36 ± 162.12^{a}	224.31 ± 171.32^{a}	215.16 ± 173.23^{a}	27.59
Pneu. height (cm)	31.59 ± 9.98^{a}	33.68 ± 5.55^{a}	23.76 ± 3.87^{c}	27.1 ± 4.37^{bc}	27.47 ± 6.50^{ab}	34.22 ± 8.58^{a}	43.13*
Pneu. volume (cm^3)	11.69 ± 4.54^{a}	12.17 ± 2.94^{a}	7.88 ± 2.00^{b}	8.89 ± 1.95^{ab}	8.87 ± 3.63^{ab}	12.66 ± 4.44^{a}	38.4*
Pneu. biomass (g)	3.74 ± 1.81^{ab}	4.73 ± 1.27^{a}	2.37 ± 0.76^{b}	3.34 ± 0.81^{ab}	4.34 ± 2.56^{a}	4.98 ± 1.90^{a}	39.2*
Nearest tree distance (m)	1.9 ± 0.91^{a}	2.3 ± 2.19^{a}	2.96 ± 2.15^{a}	2.34 ± 1.38^{a}	1.9 ± 1.26^{a}	2.44 ± 2.19^{a}	4.17
Pneu. temperature (°C)	29.97 ± 1.85^{b}	n.m	30.01 ± 1.72^{b}	n.m	34.54 ± 3.23^{a}	n.m	44.06*

Table 1. Microenvironment and morphology of pneumatophores (pneu.) from different mangrove ecotypes in Yucatan during the dry and rainy season. Data are means ± standard deviation. Letters denote significant differences between mangrove ecotypes-season combinations as resulted from the one-way ANOVA on ranks (H-values). Asterisks denote $P < 0.001$, and n.m. = not measured.

(height, volume, and biomass) were slightly higher for the rainy than for the dry seasons for all mangrove types (Table 1).

Physicochemical variables

Flooding level for the basin mangrove was always higher than for the scrub and fringe mangroves (dry season, H = 56.30; $P < 0.001$; rainy season, H = 48.32; $P < 0.001$; Fig. 2A). For the fringe mangrove, flooding level was significantly higher during the rainy season than during the dry season (Fig. 2A; $P < 0.001$).

During the dry season, the scrub mangrove had the highest mean porewater salinity (48.61 ± 2.43‰; H = 73.20; $P < 0.001$), followed by the fringe (33.69 ± 0.65‰) and the basin (17.82 ± 0.91‰) mangroves (Fig. 2B). Surface water salinity was about seven-fold higher in scrub (36.39 ± 20.01‰; H = 62.75; $P < 0.001$) than in fringe (4.53 ± 0.54‰) and in basin (5.93 ± 1.33‰) mangrove ecotypes. Porewater and surface water salinities had significant differences in basin (t = − 16.31; $P < 0.001$) and fringe (t = − 33.69; $P < 0.001$), but slight in scrub (t = − 2.75; $P = 0.020$) mangrove ecotypes.

In the rainy season, porewater and surface water salinities at the basin mangrove ecotype were significantly lower than for the fringe and the scrub mangrove ecotypes (porewater, H = 34.11; water, H = 62.75; $P < 0.001$; Fig. 2B; Table 1). However, no differences in salinity porewater were found between seasons for the basin and fringe mangroves; it only decreased significantly for the scrub mangrove in the rainy season (Fig. 2B; $P < 0.001$).

Mean temperature of the sediment was higher for the scrub mangrove than for the basin and fringe mangrove ecotypes (dry season, H = 69.36; $P < 0.001$; rainy season, H = 37.11; $P < 0.001$). This temperature was also significantly higher during the rainy season than during the dry season in the fringe mangrove ecotype (Fig. 2C; $P < 0.001$).

Pneumatophore CO_2 effluxes

Pneumatophore abundance explained up to 91% of the variation in CO_2 effluxes for the scrub, 87% for the fringe, and 83% for the basin mangrove ecotypes (Fig. 3; Table S1) during the rainy season at the water–air interface. During the dry season, when measurements were also done for the sediment-air interface, pneumatophore abundance explained up to 83% of the variation in CO_2 effluxes for scrub, 77% for basin, and 65% for fringe mangrove forests (Fig. 3; Table S1). The slope of these relationships, which denote the individual contribution of pneumatophores, were also related to the mangrove ecotype, where the steepest slopes were recorded at the fringe mangrove for sediment-air (4.51×10^{-3}) and the scrub mangrove for water–air (4.78×10^{-3}) interfaces as compared to the lower contribution of pneumatophores in basin mangrove for sediment-air (3.04×10^{-3}) and water–air (2.34×10^{-3}) interfaces (Fig. 3; Table S1). This effect was greater in the dry season (4.30×10^{-3}) than in the rainy season (3.49×10^{-3}) as well as in the sediment-air (4.54×10^{-3}) than in the water–air (3.20×10^{-3}) interface (Table S1). Overall, the highest contribution of pneumatophores to CO_2 effluxes was found in the fringe mangrove (6.24×10^{-3}; Table S1).

Biophysical associations

The CO_2 efflux at the sediment-air was mainly correlated with sediment temperature ($\rho = -0.73$), porewater salinity ($\rho = -0.45$), and pneumatophore abundance ($\rho = 0.49$; Fig. 4 top). Instead, CO_2 efflux at the water–air interface was related to pneumatophore abundance ($\rho = 0.82$) and pneumatophore height ($\rho = 0.32$; Fig. 4 bottom). Because normality's assumption was not satisfied for our data, Spearman's correlations were more convenient.

We performed a Canonical Correlation Analysis (CCA; Fig. 5) to explore the contribution of physicochemical and biological variables to the CO_2 effluxes in the three mangrove ecotypes evaluated. As categories, we

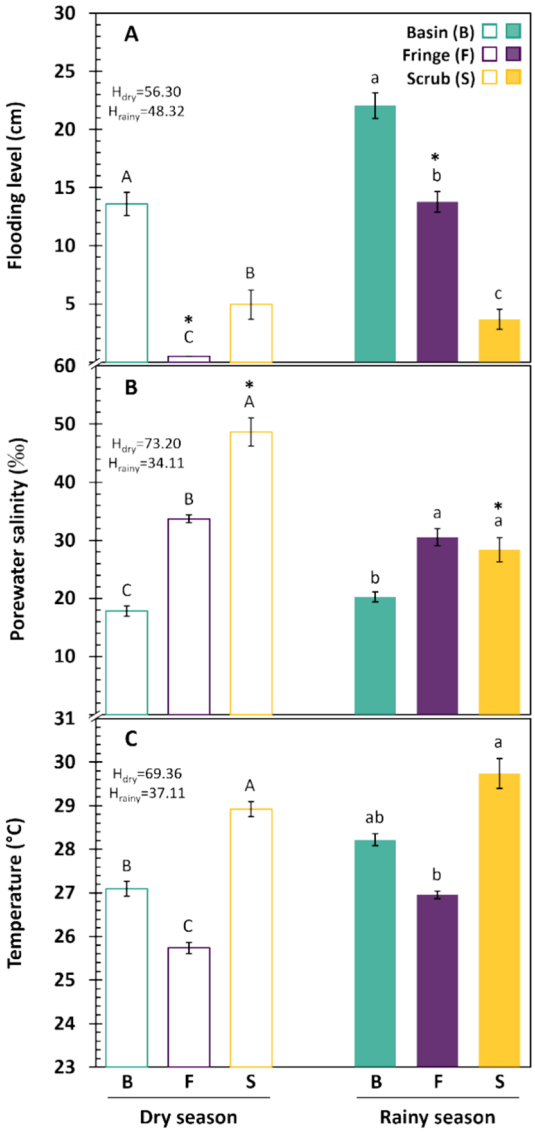

Figure 2. Flooding level (**A**), sediment porewater salinity (**B**), and temperature (**C**) of sediment (dry season) or surface water (rainy season) in the three mangrove ecotypes for the dry (open bars) and rainy (filled bars) season in Yucatan, Mexico. Data are means ± SE. Letters denote differences among mangrove ecotypes within each season (capital letters for dry and lowercase for rainy); and asterisks denote differences between seasons within mangrove ecotypes ($P < 0.001$). H-values for the Kruskal Wallis tests are given for dry (H_{dry}) and rainy (H_{rainy}) season.

used mangrove ecotype and as objects the variables measured, including the CO_2 efflux. Mangrove ecotypes were distinguished by salinity, temperature, and flood height. Surface water salinity (F2 contribution 47.36%), porewater salinity (F2 contribution 13.00%), and sediment temperature (F1 contribution 14.41%) separated scrub mangrove; flooding conditions (F1 contribution 36.90%) segregated basin mangrove; and CO_2 effluxes (F2 contribution 11.37%) separated fringe mangrove.

Temperature and salinity effects

The CO_2 effluxes were inversely correlated with sediment or water temperature (Fig. 6A) and with porewater or water salinities at the sediment-air and water–air interface, respectively (Fig. 6B). Sediment temperature was positively correlated with porewater salinity ($\rho = 0.38$; Fig. 4 top) which ultimately differentiated the mangrove ecotypes (Fig. 5). Higher temperatures were found in saline sites exposed to higher solar radiation (scrub mangrove) and lower temperatures in sites with medium to low salinities below the canopy (fringe and basin mangroves; Fig. 2B,C). Likewise, magnitudes of sediment-air CO_2 effluxes in scrub mangrove did not differ from those from the water–air interface (Fig. 3C). This mangrove ecotype was also the only one where flooding was less variable during measurements (Fig. 2A). Indeed, temperature and salinity decreased the CO_2 effluxes from pneumatophores in the three mangrove types studied.

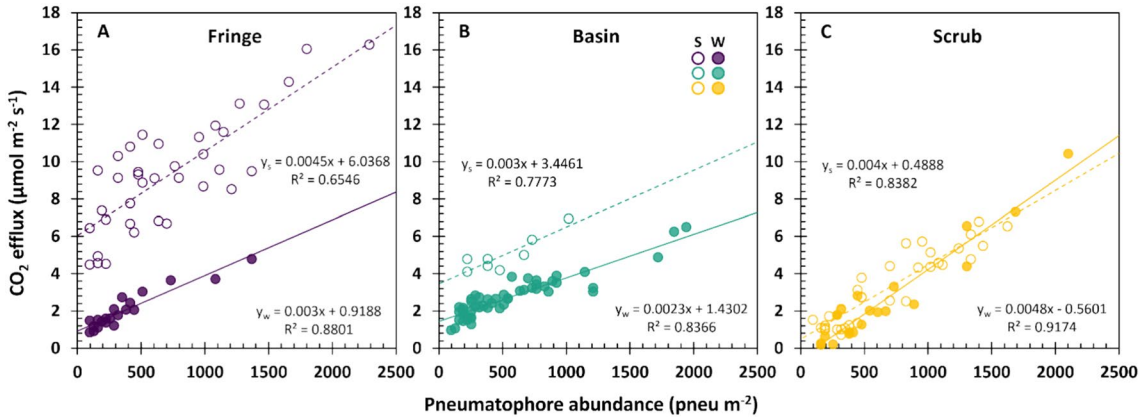

Figure 3. Linear relationships of CO_2 effluxes and pneumatophore abundance for fringe (**A**), basin (**B**) and scrub (**C**) mangrove ecotypes at sediment-air (S, open circles) and water–air (W, filled circles) interfaces.

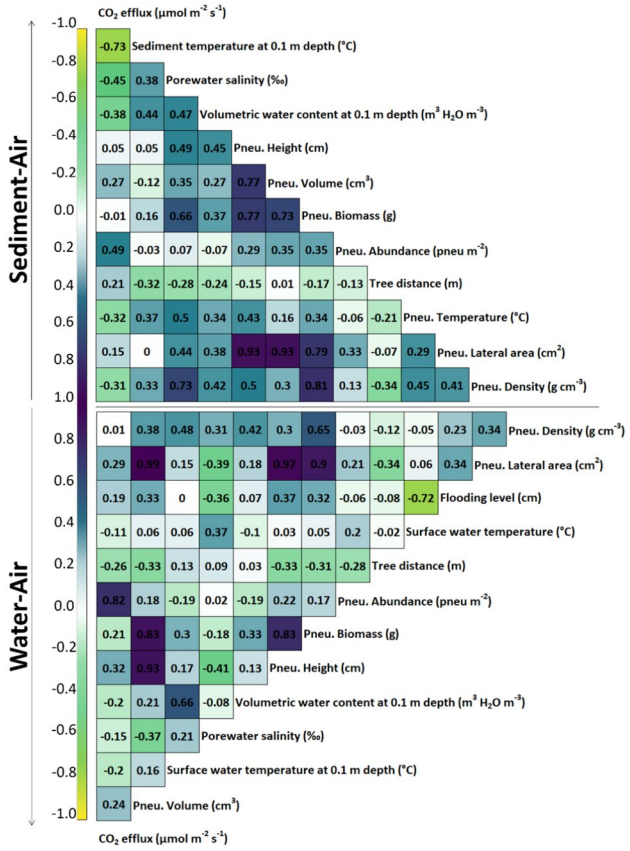

Figure 4. Correlation matrix for pair correlation of all variables using the Spearman's rank method for the sediment-air (top) and water–air (bottom) interfaces. Pneu. = Pneumatophore Some variables are not shared in both interfaces due to the absence of measurements.

Figure 6 shows the relationship between CO_2 efflux with salinity and temperature for each exchange interface. Both sediment and surface water temperatures decreased CO_2 efflux from sediment-air and water–air interfaces (Fig. 6A,B). A similar pattern is observed for porewater and surface water salinity (Figs. 6C,D, S1). Indeed, CO_2 effluxes decreased from fringe to scrub mangroves, similar to the groups formed when porewater salinity and both sediment and surface water temperatures were plotted (Fig. S2).

Interface and seasonal effects on CO_2 effluxes

Although no differences were found among mean pneumatophore abundance and mangrove ecotypes and seasons, mean CO_2 efflux varied with mangrove ecotype, interface, and season (Fig. 7). Mean pneumatophore abundance was 255.65 ± 145.37 pneu m^{-2} for basin, 254.32 ± 162.79 pneu m^{-2} for fringe and 218.41 ± 172.40 pneu

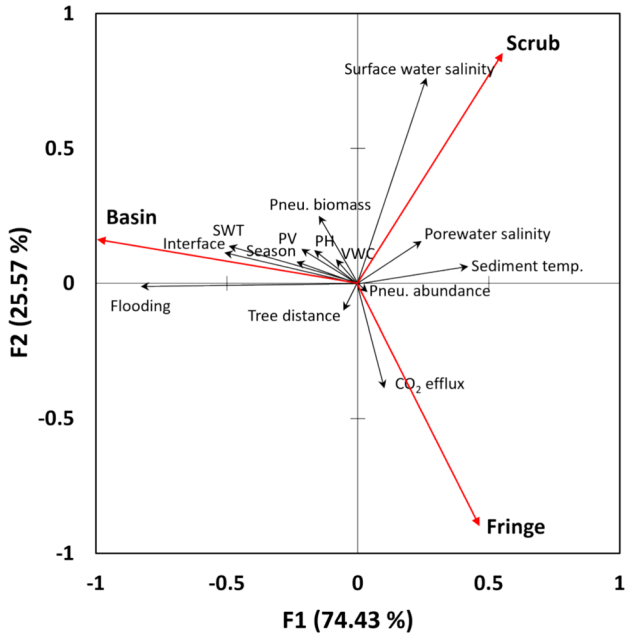

Figure 5. Canonical Correlation Analysis (CCA) of physicochemical and biological variables related to the CO_2 efflux and mangrove ecotype. Surface water temperature (SWT), pneumatophore volume (PV) and height (PH), volumetric water content (VWC).

m^{-2} for scrub during all measurements (Table 1). Differences of mean CO_2 efflux among mangrove ecotypes were given by differences in mean porewater salinity (dry season for sediment-air interface, $H = 218.46$; $P < 0.001$; rainy season for water–air interface, $H = 251.41$; $P < 0.001$). However, mean CO_2 efflux decreased either from dry to rainy season or from sediment-air to water–air due to increasing flooding levels (Figs. 2A, 7A,B). For the sediment-air interface, the highest CO_2 efflux was for the fringe mangrove (7.19 ± 0.74 µmol m^{-2} s^{-1}), and the lowest was for the scrub mangrove (1.28 ± 0.74 µmol m^{-2} s^{-1}), both during the dry season (Fig. 7A). For the water–air interface, the highest CO_2 efflux was for the basin mangrove (2.14 ± 0.24 µmol m^{-2} s^{-1}) and the lowest CO_2 efflux was for the scrub mangrove during both the dry (0.28 ± 0.83 µmol m^{-2} s^{-1}) and the rainy (0.59 ± 0.80 µmol m^{-2} s^{-1}) seasons (Fig. 7B). There was a slight increase of CO_2 efflux in the scrub mangrove from the dry to the rainy seasons in both sediment-air and water–air interfaces (Fig. 7A,B).

Discussion

Although CO_2 efflux from soils and pneumatophores of mangrove forests dominated by trees of the genus *Avicennia* has been documented[11–14], only one reports both pneumatophore abundance and mangrove ecotype[14]. These studies reported lower CO_2 effluxes than those in the present study. We found mean CO_2 effluxes rates of 1.61–7.19 µmol m^{-2} s^{-1} (with a mean pneumatophore abundance from 224.31 to 256.01 pneu m^{-2}) at the sediment-air interface, which is comparable to the mean CO_2 effluxes reported globally from mangrove soils throughout the world reported by Akhand et al.[10] (− 0.37 to 8.73 µmol m^{-2} s^{-1}). Data from creeks and estuaries surrounding mangrove forests[10,27,35] show a large range of data, from − 0.01 to 7.28 µmol m^{-2} s^{-1}, but our data from water–air interfaces, in the presence of pneumatophores, has a small range (0.51–2.05 µmol m^{-2} s^{-1}). However, the use of different methods for CO_2 measurements, as well as the large variation between mangrove ecotypes and climate conditions, do not allow us to make direct comparisons.

Even though we did not carry out measurements of sediment or water only, from the regression intercepts of Fig. 3 we can obtain basal respirations of 6.04 µmol m^{-2} s^{-1} for fringe, 3.45 µmol m^{-2} s^{-1} for basin, and 0.49 µmol m^{-2} s^{-1} for scrub mangrove ecotypes at the sediment-air interface; and 0.92, 1.43 and − 0.56 µmol m^{-2} s^{-1} from fringe, basin, and scrub mangroves, respectively, at the water–air interface. Then, we can consider that the proportion of aerial autotrophic respiration can be comparable to those CO_2 effluxes from sediments or water with pneumatophores minus that basal efflux. Autotrophic respiration is supposed to represent 48.60% of the total soil respiration in forests[36]. In our study, this proportion would be of 15.62–69.69% and 30.15–209.13% for sediment-air and water–air, respectively, and taking into consideration the CO_2 release driven by pneumatophores only. Yet, although *Avicennia* is one of the most widely distributed mangrove genera and can have more than 10,000 pneumatophores per tree[37,38], pneumatophore CO_2 effluxes are not being reported as a distinct form of carbon loss in mangroves[39].

As predicted, CO_2 effluxes were greater at high pneumatophore abundance, which is related to a high plant biomass. When soils are flooded, pneumatophore respiration is supposed to be the main source of CO_2 effluxes, because gas diffusion in the water column is limited. Additionally, the individual contribution of the pneumatophores is represented by the slope value of the relationships between CO_2 efflux and pneumatophore abundance,

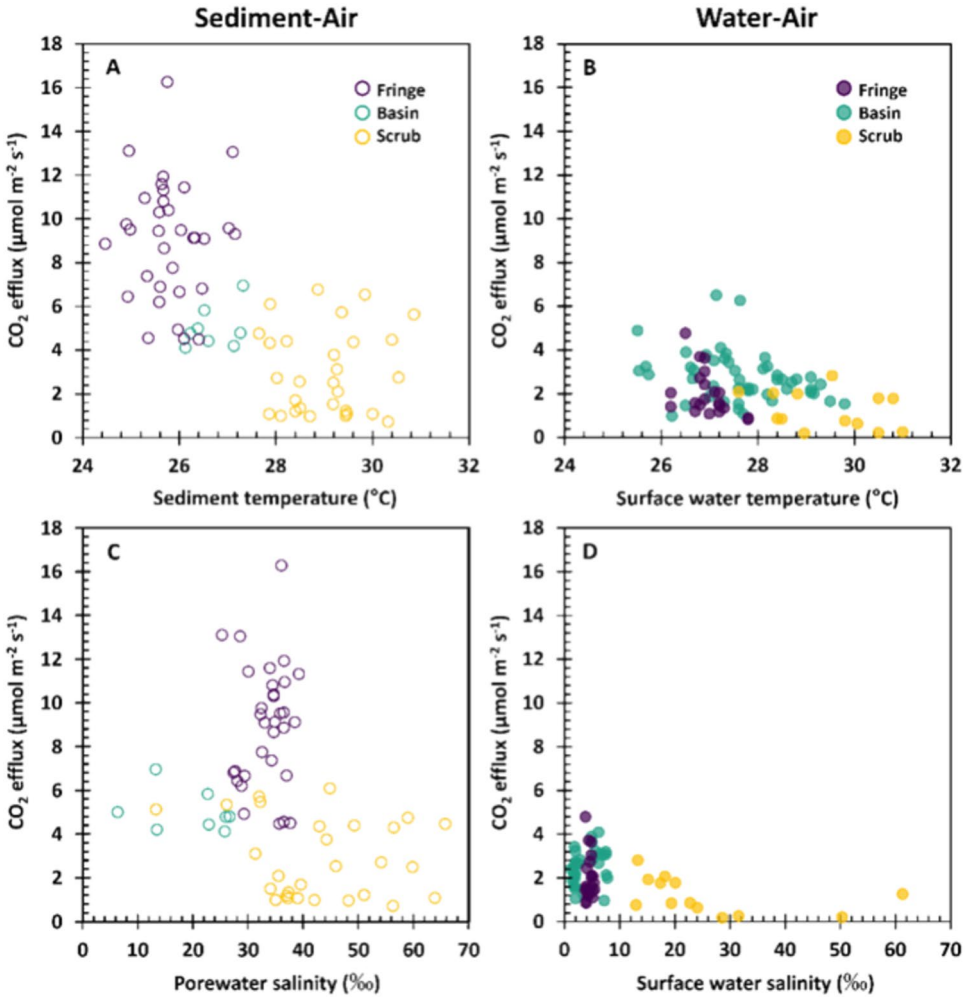

Figure 6. Relationships between pneumatophore CO_2 effluxes and sediment temperature (**A**), surface water temperature (**B**), porewater salinity (**C**) and surface water salinity (**D**) from both sediment-air (open circles, left panels) and water–air (filled circles, right panels) interfaces.

allowing comparisons between mangrove ecotypes or tree ages. Pneumatophore CO_2 effluxes were greater at the sediment-air than at the water–air interface exchange for the fringe and basin mangrove ecotypes. For the scrub mangrove, such regressions showed data points overlapping from both interfaces (Fig. 3C), but mean CO_2 effluxes were higher at the sediment-air than at the water–air interface for both seasons (Fig. 7A,B; Fig. S3). Hydrodynamics in mangrove forests depends on the duration, level, and frequency of flooding, and it is known that CO_2 increases during ebb and spring tides and decreases during flow and neap tides[27]. In our study, we only tested the presence (level) or absence of the water column and found that passing from sediment-air to water–air conditions, the CO_2 efflux rates decreased 76.77%, 49.75% and 68.32% for fringe, basin, and scrub mangrove ecotypes. These results can help adjust our current CO_2 models in mangrove forests, considering their hydrology.

Under sunlight, flooding can also reduce CO_2 fixation by photosynthetic layers of pneumatophores in *Avicennia marina*[24]. In preliminary studies we found that 35.36 ± 28.22% of the respired CO_2 is offset by pneumatophore photosynthesis (unpublished data), like the 49.58 ± 13.35% observed in *A. officinalis* and *Sonneratia alba*[40]. Thus, pneumatophore photosynthesis can represent a source of oxygen and carbon when leaf stomata are closed at high vapor pressure deficit especially for the scrub mangrove ecotype, allowing survival during the dry season.

Few studies have reported CO_2 effluxes as a function of salinity variability within the same mangrove ecotype[10,13]. It is well known that salinity decreases photosynthesis and respiration in plants[33,34,41–43], accordingly, the site with the highest salinity (scrub ecotype) had the lowest CO_2 effluxes despite its high sediment and surface water temperatures. This was unexpected, as typically high temperatures increase respiration[34]. In this study, the scrub ecotype showed lower CO_2 efflux during both dry and rainy seasons (Fig. 7), suggesting that high salinity also reduces soil respiration[44]. In fact, in our study, the CO_2 efflux was the result of the effect of salinity, temperature, and flooding that differed between mangrove ecotypes (Figs. 2, 6; Fig. S2). Although the basin mangrove had the lowest porewater salinities, it showed low CO_2 effluxes because it had the highest flooding level; however, during the dry season in non-flooded places, CO_2 effluxes were high (Table S1, Fig. 7). Also, during the dry season, flooding level was inversely correlated with sediment temperature and pneumatophore temperature, which reduced CO_2 efflux. In studies conducted in soils of different forests, a positive relationship

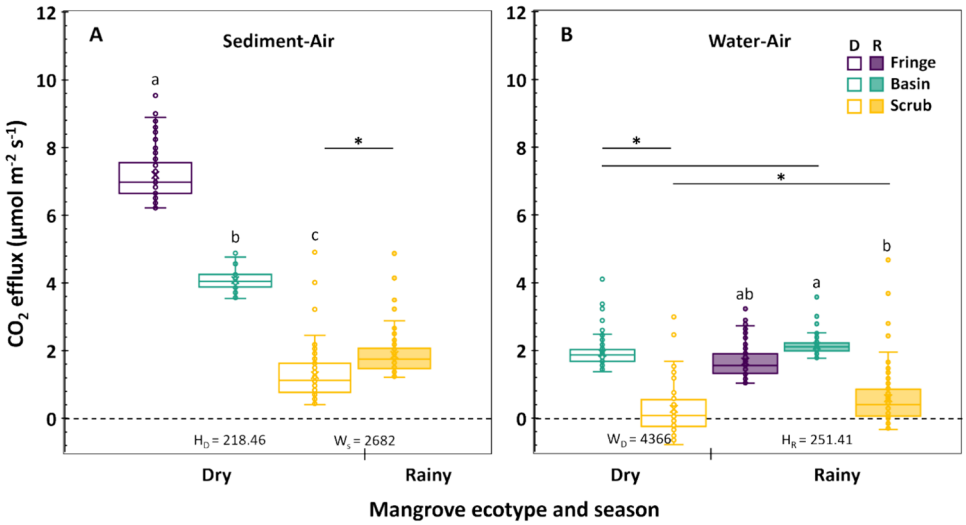

Figure 7. Median CO_2 effluxes from three different mangrove ecotypes during the dry (open boxes) and rainy (filled boxes) seasons at the sediment-air (**A**) and water–air (**B**) interfaces. Boxes correspond from first to third quartiles; letters denote significant differences among mangrove ecotypes, capital letters for sediment-air and lowercase for water–air interfaces. Lines and asterisks denote differences between seasons for the same mangrove ecotype (**A**) or between mangrove ecotypes within seasons (**B**; $P < 0.01$).

between CO_2 effluxes and soil temperature has been found[7,8], because high temperatures favor microbial activity in the soil[33]. However, in our study, an interaction between high temperatures and high salinities led to a lower CO_2 efflux in the scrub mangrove forest for both seasons and both exchange interfaces.

Mangrove soils that are rich in carbon, organic matter, and nutrient availability (e.g., N, P and Fe) favor CO_2 efflux[9,45]. In some mangrove flooded soils, the enzyme that regulates phosphorus (P) cycling (alkaline phosphatase) is strongly related to CO_2 effluxes, but no relationship between the enzyme that regulates nitrogen (N) cycling (β-N-acetylglucosaminidase) and CO_2 efflux was found[46]. Lower CO_2 effluxes in the scrub mangrove forest could then indicate that this site is P-limited, because previous reports assign the stature of this mangrove forests to P deficiency in soils[47–49], although this is still controversial[50]. In our study, the CO_2 effluxes in flooded soils of scrub mangroves were like those in non-flooded soils and, in some cases, these were very low or even negative values (Figs. 2C, 7). Further research on salinity and P availability would also be needed in arid regions, where scrub mangroves are dominated by *Avicennia germinans*[51].

During the rainy season, we found the tallest pneumatophores in all mangrove forests because of a higher level and frequency of flooding events[29] and confirmed a positive correlation between pneumatophore height and flooding level ($\rho = 0.48$; Fig. 3). Pneumatophore height has also been positively correlated to flooding level in several studies[52–54], and both pneumatophore height and density have been reported as indicators of soil and hydrodynamics conditions in mangroves[37,54]. Pneumatophores of *Avicennia* spp. are supposed to be up to 30 cm in height[38], but, in our study, pneumatophores were up to 48 cm in height in the scrub mangrove ecotype. This pneumatophore's extreme length can be related to the increase in water level due to the heavy rain caused by four tropical storms in 2020 in the Yucatan Peninsula[55].

The average CO_2 effluxes from *A. germinans* pneumatophores in our study sites, at the water–air and sediment-air interfaces, were comparable to those reported in several studies[11,44,56,57]. The highest CO_2 effluxes in this study were even higher than those from other forest ecosystems around the world [58–62], reflecting the high productivity of the mangrove ecosystems. Our findings question the current understanding of the carbon budget in mangrove forests and highlight the importance of considering integrating physiology and anatomy within carbon-based studies. Indeed, we propose that further studies on CO_2 (or other greenhouse gases) effluxes should also consider other mangrove tissues, such as stilts, stems, and even leaves, to evaluate their contribution to ecosystem respiration under different global change scenarios.

Materials and methods

Study sites and field measurements

Three mangrove ecotypes, dominated by *Avicennia germinans* (L.) L. were chosen in the northwestern coast of Yucatan: fringe and basin mangroves in the Ria Celestun Biosphere Reserve (20° 51′ 27.4″ N, – 90° 22′ 33.9″ W; 20° 51′ 03.6″ N, – 90° 17′ 42.5″ W, respectively; Ramsar Site 1333; Fig. 1) and scrub mangrove in the State Reserve Cienagas y Manglares de la Costa Norte de Yucatán (21° 13′ 17.7″ N, – 89° 49′ 49.4″ W; Ramsar Site 2468; Fig. 1). Field measurements were made in May 2021 and in September 2021 for the dry and rainy seasons, respectively. Sediment-air and/or water–air interfaces were considered depending on the inundation state of each mangrove ecotype on the day of measurements. When possible, both interfaces were measured. Sediment-air interface was measured for all mangrove ecotypes during the dry season and only for scrub mangrove forests during the rainy

season. The water–air interface was evaluated for all mangrove ecotypes during the rainy season, and for basin and scrub mangroves during the dry season.

Physicochemical measurements

Air temperature and relative humidity were recorded with a 12-bit Temp/RH Smart Sensor (S-THB-M002, Onset Computer Corporation, Bourne, MA) every 10 s, and 10-min averages were stored with a data acquisition system (HOBO U30-NRC Weather Station, Onset) at each mangrove ecotype during the fieldwork in both seasons. Porewater samples were taken at 30 cm soil depth adjacent to each CO_2 efflux tube, then porewater salinity was measured. When sediment was flooded, surface water salinity, surface water temperature and flooding level were taken. Both porewater and surface water parameters were obtained with a portable conductivity meter (YSI, Model Pro2030, Yellow Springs, OH). Porewater salinity was measured in all cases for both sediment-air and water–air CO_2 efflux measurements. Sediment temperature (Type "T" Omega Soil Temperature Probe, Omega Engineering Inc., Stamford, CT) and volumetric water content (Theta Probe ML2x, The Macaulay Land Use Research Institute and Delta T Devices, Cambridge, UK) were recorded at 0.1 m depth of the sediment next to each PVC tube at the same time as CO_2 efflux was being measured for non-flooded conditions, while surface water temperature was measured for flooded conditions. During the dry season, we also measured pneumatophore temperature (Table 1).

Pneumatophores characterization

At each mangrove ecotype and season, 32–37 plots (0.5 m^2 each; divided into 4 subplots) were randomly chosen for pneumatophores counting to estimate the mean pneumatophore abundance per unit area (pneu m^{-2}; Table 1). Within each plot a polyvinyl chloride (PVC) tube (0.2 m diameter, and 0.30 ± 0.08 m height) was inserted 0.03 m into the sediment. PVC tubes were placed at each site before CO_2 efflux measurements were taken. To represent different pneumatophore abundances, PVC tubes were placed enclosing from 3 to 72 pneumatophores each, which cover pneumatophore abundances ranging from 95 to 2292 pneu m^{-2} (Fig. 3). Additionally, the distance from the PVC tube to the nearest tree was also taken. After CO_2 efflux measurements, five pneumatophores per PVC tube were characterized in the field measuring total height, basal diameter, top diameter, and distance between the top diameter and apex of the pneumatophores. Three pneumatophores per PVC tube were taken to the laboratory to obtain pneumatophore-dried biomass (g). Then, pneumatophore basal area (cm^2), lateral area (cm^2), total volume (cm^3), and density (g cm^{-3}) were calculated.

CO_2 efflux measurements

CO_2 efflux rates from pneumatophores or sediment-air and water–air were quantified using a dynamic-closed chamber system (0.2 m in diameter: 8200–103 Smart Chamber, LI-COR Biosciences; Lincoln, NE) connected to an infrared gas analyzer (LI-8100A, LI-COR). For each sampling point, chambers were placed on PVC tubes previously installed (one week before), and then CO_2 efflux was recorded for 7 min. At each season, CO_2 efflux measurements were made from 8:30 to 12:30 h. The CO_2 efflux data were first analyzed using the SoilFlux Pro-4.2.1 software (LI-COR Biosciences) to recognize possible leaks or disturbances inside the chamber during measurements. Then, effluxes were re-computerized using asymptotic fits, previously employed for soils, plants, and waters to reduce underestimations[63–65]. Only fits with an $R^2 \geq 0.95$ were chosen (n = 171).

Data analysis and representation

Normality (Shapiro–Wilk) and homoscedasticity (Levene) were tested for all data before parametric analysis. Then, simple regressions were run to elucidate the relationship between pneumatophores abundance and CO_2 effluxes by mangrove ecotype, season, interface, and its interactions (Fig. 3; see Supplementary Table S1). Kruskal–Wallis (or one-way ANOVA on ranks) analyses were performed to find differences among mangrove ecotypes within each interface or season, then reported as H-values (Table 1; Figs. 2, 7). Also, Mann–Whitney-Wilcoxon were performed to test two groups' differences for ecotype or season, then reported as W-values (Fig. 7). For pairwise multiple comparisons either Dunn's or Tukey's procedures with or without Bonferroni or Holm adjustments were used. Analysis for Figs. 3, 4 and Table S1 were made from raw field data (n = 171). To elucidate the role of biophysical variables, a multi-comparison matrix using Spearman's correlation was performed. To account for the contribution of physicochemical and biological variables to the CO_2 efflux and the differentiation of mangrove ecotypes, a Canonical Correspondence Analysis (CCA) was used. Models from Table S1 and Fig. 3 were applied to the pneumatophore abundance dataset (from characterization), and then it was unified with the CO_2 efflux dataset containing only CO_2 effluxes from the mean pneumatophore abundance observed at each mangrove ecotype, to exclude outliers. This new dataset from observed and predicted data was used for Fig. 7 (totaling n = 850). All statistical analyses were performed using R language version 2023.03.1.446[66]. Results are usually presented in terms of the mean ± standard error, unless specified.

Data availability

Data will be made available on request to any of the correspondent authors.

Received: 15 December 2023; Accepted: 29 July 2024
Published online: 08 August 2024

References

1. Bouillon, S. *et al.* Mangrove production and carbon sinks: A revision of global budget estimates. *Glob. Biogeochem. Cycles* **22**, GB2013. https://doi.org/10.1029/2007GB003052 (2008).

2. Donato, D. C. *et al.* Mangroves among the most carbon-rich forests in the tropics. *Nat. Geosci.* **4**, 293. https://doi.org/10.1038/ngeo1123 (2011).
3. Friess, D. A., Adame, M. F., Adams, J. B. & Lovelock, C. E. Mangrove forests under climate change in a 2 °C world. *WIREs Clim. Change* **13**(4), e792. https://doi.org/10.1002/wcc.792 (2022).
4. Leal, M. & Spalding, M. D. (eds.). The State of the World's Mangroves 2022. Global Mangrove Alliance, 92 p (2022).
5. de Gerenyu, L. *et al.* Daily and seasonal dynamics of CO_2 fluxes from soils under different stands of monsoon tropical forest. *Eurasian Soil Sci.* **44**(9), 984–990. https://doi.org/10.1134/S1064229311090067 (2011).
6. Leon, E. *et al.* Hot spots, hot moments, and spatio-temporal controls on soil CO_2 efflux in a water-limited ecosystem. *Soil Biol. Biochem.* **77**, 12–21. https://doi.org/10.1016/j.soilbio.2014.05.029 (2014).
7. Lovelock, C. E. Soil respiration and belowground carbon allocation in mangrove forests. *Ecosystems* **11**, 342–354. https://doi.org/10.1007/s10021-008-9125-4 (2008).
8. Poungparn, S. *et al.* Carbon dioxide emission through soil respiration in a secondary mangrove forest of eastern Thailand. *J. Trop. Ecol.* **25**(4), 393–400 (2009).
9. Chen, G., Tam, N. & Ye, Y. Spatial and seasonal variations of atmospheric N_2O and CO_2 fluxes from a subtropical mangrove swamp and their relationships with soil characteristics. *Soil Biol. Biochem.* **48**, 175–181. https://doi.org/10.1016/j.soilbio.2012.01.029 (2012).
10. Akhand, A., Chanda, A., Das, S., Hazra, S. & Kuwae, T. CO_2 fluxes in mangrove ecosystems. In *Blue carbon in shallow coastal ecosystems, carbon dynamics, policy, and implementation* (eds Kuwae, T. & y Hori, M.) 185–221 (Springer, Singapore, 2019). https://doi.org/10.1007/978-981-13-1295-3_7.
11. Kristensen, E. *et al.* Emission of CO_2 and CH_4 to the atmosphere by sediments and open waters in two Tanzanian mangrove forests. *Mar. Ecol. Prog. Ser.* **370**, 53–67. https://doi.org/10.3354/meps07642 (2008).
12. Penha-Lopes, G. *et al.* The role of biogenic structures on the biogeochemical functioning of mangrove constructed wetlands sediments—A mesocosm approach. *Mar. Pollut. Bull.* **60**(4), 560–572. https://doi.org/10.1016/j.marpolbul.2009.11.008 (2010).
13. Troxler, T. G. *et al.* Component-specific dynamics of riverine mangrove CO_2 efflux in the Florida coastal Everglades. *Agric. For. Meteorol.* **213**, 273–282. https://doi.org/10.1016/j.agrformet.2014.12.012 (2015).
14. Kristensen, E. *et al.* Pneumatophores and crab burrows increase CO_2 and CH_4 emission from sediments in two Brazilian fringe mangrove forests. *Mar. Ecol. Prog. Ser.* **698**, 29–39. https://doi.org/10.3354/meps14153 (2022).
15. Nie, S. *et al.* Sediment CO_2 flux from a mangrove in southern China: Is it controlled by spatiotemporal, biotic or physical factors?. *Forests* **14**, 782. https://doi.org/10.3390/f14040782 (2023).
16. Purjava, R., Ramesh, R. & Frenzel, P. Plant-mediated methane emission from an Indian mangrove. *Glob. Change Biol.* **10**, 1825–1834. https://doi.org/10.1111/j.1365-2486.2004.00834.x (2004).
17. Krithika, K., Purjava, R. & Ramesh, R. Fluxes of methane and nitrous oxide from an Indian mangrove. *Curr. Sci.* **94**(2), 218–224 (2008).
18. Lin, C. W., Kao, Y. C., Lin, W. J., Ho, C. W. & Lin, H. J. Effect of pneumatophore density on methane emissions in mangroves. *Forests* **12**, 314. https://doi.org/10.3390/f12030314 (2021).
19. Sheng, N., Wu, F., Liao, B. & Xin, K. Methane and carbon dioxide emissions from cultivated and native mangrove species in Dongzhai Harbor, Hainan. *Ecol. Eng.* https://doi.org/10.1016/j.ecoleng.2021.106285 (2021).
20. Zhang, C. *et al.* Massive methane emission from tree stems and pneumatophores in a subtropical mangrove wetland. *Plant Soil* **473**, 489–505. https://doi.org/10.1007/s11104-022-05300-z (2022).
21. Purnobasuki, H. & Suzuki, M. Aerenchyma tissue development and gas-pathway structure in root of *Avicennia marina* (Forsk.) Vierh. *J. Plant Res.* **118**(4), 285–294. https://doi.org/10.1007/s10265-005-0221-7 (2005).
22. Purnobasuki, H., Purnama, P. R. & Kobayashi, K. Morphology of four root types and anatomy of root-root junction in relation gas pathway of *Avicennia marina* (Forsk) Vierh roots. *Vegetos* https://doi.org/10.5958/2229-4473.2017.00143.4 (2017).
23. Yánez-Espinosa, L. & Ángeles, G. Does mangrove stem bark have an internal pathway for gas flow?. *Trees* **36**, 361–377. https://doi.org/10.1007/s00468-02102210-y (2022).
24. Aiga, I., Nakano, Y., Ohki, S., Kitaya, Y. & Yabuki, K. Photosynthetic CO_2 fixation in pneumatophores of gray mangrove. *Avicennia marina. Environ. Control Biol.* **33**(2), 97. https://doi.org/10.2525/ecb1963.33.97 (1995).
25. Kitaya, Y. *et al.* Gas Exchange and oxygen concentration in pneumatophores and prop roots of four mangrove species. *Trees* **16**, 155–158. https://doi.org/10.1007/s00468-002-0167-5 (2002).
26. Lin, C. W. *et al.* Methane emissions from subtropical and tropical mangrove ecosystems in Taiwan. *Forests* **11**, 470. https://doi.org/10.3390/f11040470 (2020).
27. Jacotot, A., Marchand, C. & Allenbach, M. Tidal variability of CO_2 and CH_4 emissions from the water column within a *Rhizophora* mangrove forest (New Caledonia). *Sci. Total Environ.* **631–632**, 334–340. https://doi.org/10.1016/j.scitotenv.2018.03.006 (2018).
28. Lugo, A. E. & Snedaker, S. C. The ecology of mangroves. *Annu. Rev. Ecol. Syst.* **5**, 39–64. https://doi.org/10.1146/annurev.es.05.110174.000351 (1974).
29. Zaldívar-Jiménez, *et al.* Conceptual framework for mangrove restoration in the Yucatán Peninsula. *Ecol. Restor.* **28**, 3. https://doi.org/10.3368/er.28.3.333 (2010).
30. Adame, M. F. *et al.* Root biomass and production of mangroves surrounding a karstic oligotrophic coastal lagoon. *Wetlands* **34**, 479488. https://doi.org/10.1007/s13157-014-0514-5 (2014).
31. Herrera-Silveira, J. A. *et al.* Blue carbon of Mexico, carbon stocks and fluxes: A systematic review. *PeerJ* **8**, e8790. https://doi.org/10.7717/peerj.8790 (2020).
32. Velázquez-Salazar et al. Manglares de México. Actualización y análisis de los datos 2020. Comisión Nacional para el Conocimiento y Uso de la Biodiversidad. México CDMX, 168 (2021).
33. Luo, Y. & Zhou, X. *Soil Respiration and the Environment* (Elsevier, Burlington, 2006). https://doi.org/10.1016/B978-0-12-088782-8.X5000-1.
34. Lambers, H. & Oliveira, R. S. *Plant Physiological Ecology* 3rd edn, 736 (Springer, Cham, 2019).
35. Call, M. *et al.* Spatial and temporal variability of carbon dioxide and methane fluxes over semi-diurnal and spring–neap–spring timescales in a mangrove creek. *Geochim. Cosmochim. Acta* **150**, 211–225. https://doi.org/10.1016/j.gca.2014.11.023 (2015).
36. Hanson, P. J., Edwards, N. T., Garten, C. T. & Andrews, J. A. Separating root and soil microbial contributions to soil respiration: A review of methods and observations. *Biogeochemistry* **48**, 115–146. https://doi.org/10.1023/A:1006244819642 (2000).
37. Tomlinson, P. B. *The Botany of Mangroves* 2nd edn, 418 (Cambridge University Press, Cambridge, 2016).
38. Chen, L. Pneumatophores. In *Encyclopedia of Estuaries. Encyclopedia of Earth Sciences Series* (ed. Kennish, M. J.) (Springer, Dordrecht, 2016). https://doi.org/10.1007/978-94-017-8801-4_282.
39. Adame, M. F. *et al.* Deconstructing the mangrove carbon cycle: Gains, transformation, and losses. *Ecosphere* **15**(3), e4806. https://doi.org/10.1002/ecs2.4806 (2024).
40. Yabuki, K. Gas exchange between the pneumatophores and roots of mangroves by photosynthesis of pneumatophore. in *Photosynthetic Rate and Dynamic Environment*. https://doi.org/10.1007/978-94-017-2640-5_5 (Springer, Dordrecht, 2004).
41. Kozlowski, T. Responses of woody plants to flooding and salinity. *Tree Physiol. Monogr.* https://doi.org/10.1093/treephys/17.7.490 (1997).

42. Medina, E. Mangrove physiology: the challenge of salt, heat, and light stress under recurrent flooding, pp. 109–126. in *Ecosistemas de Manglar en América Tropical* (ed. Yáñez-Arancibia, A., Lara-Domínguez, A. L.) 380 (Instituto de Ecología A.C. México, Costa Rica, 1999).
43. Krauss, K. W. *et al.* Environmental drivers in mangrove establishment and early development: A review. *Aquat. Bot.* **89**, 105–127. https://doi.org/10.1016/j.aquabot.2007.12.014 (2008).
44. Kristensen, E., Bouillon, S., Dittmar, T. & Marchand, C. Organic carbon dynamics in mangrove ecosystems: A review. *Aquat. Bot.* **89**, 201–219. https://doi.org/10.1016/j.aquabot.2007.12.005 (2008).
45. Chen, G. C., Tam, N. F. Y. & Ye, Y. Summer fluxes of atmospheric greenhouse gases N_2O, CH_4 and CO_2 from mangrove soil in South China. *Sci. Total Environ.* **408**(13), 2761–2767. https://doi.org/10.1016/j.scitotenv.2010.03.007 (2010).
46. Chambers, L., Guevara, R., Boyer, J. N., Troxler, T. & Davis, S. E. Effects of salinity and inundation on microbial community structure and function in a mangrove peat soil. *Wetlands* **36**, 361–371. https://doi.org/10.1007/s13157-016-0745-8 (2016).
47. Feller, O. C., McKee, K. L., Whigham, D. F. & O'Neill, J. P. Nitrogen vs. phosphorus limitation across an ecotonal gradient in a mangrove forest. *Biogeochemistry* **62**, 145–175. https://doi.org/10.1023/A:1021166010892 (2003).
48. Lovelock, C. E., Feller, I. C., McKee, K. L., Engelbrechts, M. L. & Ball, M. C. The effect of nutrient enrichment on growth, photosynthesis and hydraulic conductance of dwarf mangroves in Panama. *Funct. Ecol.* **18**, 25–33. https://doi.org/10.1046/j.0269-8463.2004.00805.x (2004).
49. Medina, E., Cuevas, E. & Lugo, A. E. Nutrient relations of dwarf *Rhizophora mangle* L. mangroves on peat in eastern Puerto Rico. *Plant Ecol.* **207**, 13–24. https://doi.org/10.1007/s11258-009-9650-z (2010).
50. Cisneros de la Cruz, D. J. *et al.* Short-distance barriers affect genetic variability of *Rhizophora mangle* L. in the Yucatan Peninsula. *Ecol. Evol.* **8**, 11083–11099. https://doi.org/10.1002/ece3.4575 (2018).
51. Adame, M. F. *et al.* Mangroves in arid regions: Ecology, threats, and opportunities. *Estuar. Coast. Shelf Sci.* https://doi.org/10.1016/j.ecss.2020.106796 (2021).
52. Toma, T., Nkamura, K., Patanaponpaiboon, P. & Ogino, K. Effect of flooding water level and plant density on growth of pneumatophore of *Avicennia marina*. *Tropics* **1**, 75–82. https://doi.org/10.3759/tropics.1.75 (1991).
53. Dahdouh-Guebas, F., Kairo, J. G., De Bondt, R. & Koedam, N. Pneumatophore height and density in relation to microtopography in the grey mangrove *Avicennia marina*. *Belg. J. Bot.* **140**(2), 213–221 (2007).
54. Al-Khayat, J. A. & Alatalo, J. M. Relationship between tree size, sediment mud content, oxygen levels, and pneumatophore abundance in the mangrove tree species *Avicennia Marina* (Forssk) Vierh. *J. Mar. Sci. Eng.* **9**, 100. https://doi.org/10.3390/jmse9010100 (2021).
55. Romero, D. & León-Cruz, J. F. Spatiotemporal changes in hurricane-force wind risk assessment in the Yucatan Peninsula, Mexico. *Nat. Hazards* https://doi.org/10.1007/s11069-023-06397-w (2024).
56. Penha-Lopes, G. *et al.* Organic carbon dynamics in a constructed mangrove wastewater wetland populated with benthic fauna: a modelling approach. *Ecol. Model.* https://doi.org/10.1016/j.ecolmodel.2012.02.005 (2012).
57. Nóbrega, G. N. *et al.* Edaphic factors controlling summer (rainy season) greenhouse gas emissions (CO_2 and CH_4) from semiarid mangrove soils (NE-Brazil). *Sci. Total Environ.* **542**, 685–693. https://doi.org/10.1016/j.scitotenv.2015.10.108 (2016).
58. Litton, C. M., Giardina, C. P., Albano, J. K., Long, M. S. & Asner, G. P. The magnitude and variability of soil-surface CO_2 efflux increase with mean annual temperature in Hawaiian tropical montane wet forests. *Soil Biol. Biochem.* **2011**(43), 2315–2323. https://doi.org/10.1016/j.soilbio.2011.08.004 (2011).
59. Katayama, A. *et al.* Effect of forest structure on the spatial variation in soil respiration in a Bornean tropical rainforest. *Agric. For. Meteorol.* **149**, 1666–1673. https://doi.org/10.1016/j.agrformet.2009.05.007 (2009).
60. Krauss, K. W. & Whitbeck, J. L. Soil greenhouse gas fluxes during wetland forest retreat along the lower Savannah River, Gerogia (USA). *Wetlands* **32**, 73–81. https://doi.org/10.1007/s13157-011-0246-8 (2012).
61. Arellano-Martín, F., Dupuy, J. M., Us-Santamaría, R. & Andrade, J. L. Soil CO_2 efflux fluctuates in three different annual seasons in a semideciduous tropical forest in Yucatan, Mexico. *Terra Latinoam.* **40**, e968. https://doi.org/10.28940/terra.v40i0.968 (2022).
62. Maher, D. T., Cowley, K., Santos, I. R., Macklin, P. & Eyre, B. D. Methane and carbon dioxide dynamics in a subtropical estuary over a diel cycle: Insights from automated in situ radioactive and stable isotope measurements. *Mar. Chem.* **168**, 69–79. https://doi.org/10.1016/j.marchem.2014.10.017 (2015).
63. Pedersen, A. R., Petersen, S. O. & Schelde, K. A comprehensive approach to soil atmosphere trace-gas flux estimation with static chambers. *Eur. J. Soil Sci.* **61**(6), 888–902. https://doi.org/10.1111/j.1365-2389.2010.01291.x (2010).
64. Pihlatie, M. K. *et al.* Comparison of static chambers to measure CH_4 emissions from soils. *Agric. For. Meteorol.* **171–172**, 124–136. https://doi.org/10.1016/j.agrformet.2012.11.008 (2013).
65. Salas-Rabaza, J. A. *et al.* Impacts of leaks and gas accumulation on closed chamber methods for measuring methane and carbon dioxide fluxes from tree stems. *Sci. Total Environ.* https://doi.org/10.1016/j.scitotenv.2023.166358 (2023).
66. Posit Team. RStudio: Integrated Development Environment for R. Posit Software, PBC, Boston. http://www.posit.co/ (2023).

Acknowledgements

We thank Gisela Mayora, Karina González, Jesús Garrido and Juan Andrés for fieldwork support. We are grateful to Frédéric Thalasso for his comments on the earliest version of the manuscript. We also thank the authorities of the Comisión Nacional de Áreas Naturales Protegidas (CONANP) for help to do field work in Celestún and Chuburná.

Author contributions

J.A.S.R. and J.L.A. conceived the study; wrote the manuscript. L.Y.E., E.C., and J.L.A. conceptualization, methodology, supervision. J.A.S.R, G.C.A., and R.U.S. organized and conducted field sampling. J.A.S.R. and J.L.A. analyzed the data. All authors reviewed the manuscript.

Funding

This research was partially supported by the International Tropical Timber Organization (ITTO) (Fellowship's number 050/20A to J.A.S.R.). J.A.S.R. and G.C.A. received a fellowship from Consejo Nacional de Humanidades, Ciencias y Tecnologías (CONAHCYT).

Competing interests

The authors declare no competing interests.

Additional information

Supplementary Information The online version contains supplementary material available at https://doi.org/10.1038/s41598-024-68822-9.

Correspondence and requests for materials should be addressed to J.L.A.

Reprints and permissions information is available at www.nature.com/reprints.

Publisher's note Springer Nature remains neutral with regard to jurisdictional claims in published maps and institutional affiliations.